AIP | The Journal of Chemical Physics

Vibrationally resolved NEXAFS at C and N K-edges of pyridine, 2-fluoropyridine and 2,6-difluoropyridine: A combined experimental and theoretical assessment

Alberto Baiardi, Marco Mendolicchio, Vincenzo Barone, Giovanna Fronzoni, Gustavo Adolfo Cardenas Jimenez, Mauro Stener, Cesare Grazioli, Monica de Simone, and Marcello Coreno

Citation: The Journal of Chemical Physics **143**, 204102 (2015); doi: 10.1063/1.4935715
View online: http://dx.doi.org/10.1063/1.4935715
View Table of Contents: http://scitation.aip.org/content/aip/journal/jcp/143/20?ver=pdfcov
Published by the AIP Publishing

Vibrationally resolved NEXAFS at C and N K-edges of pyridine, 2-fluoropyridine and 2,6-difluoropyridine: A combined experimental and theoretical assessment

Alberto Baiardi,[1] Marco Mendolicchio,[1] Vincenzo Barone,[1,a)] Giovanna Fronzoni,[2] Gustavo Adolfo Cardenas Jimenez,[2] Mauro Stener,[2] Cesare Grazioli,[2] Monica de Simone,[3] and Marcello Coreno[4]

[1]*Scuola Normale Superiore, Piazza dei Cavalieri 7, 56125 Pisa, Italy*
[2]*Dipartimento di Scienze Chimiche e Farmaceutiche, Universita' di Trieste, Via Giorgieri 1, 34127 Trieste, Italy*
[3]*CNR-IOM, Laboratorio TASC, Area Science Park Basovizza, 34149 Trieste, Italy*
[4]*CNR-ISM, UOS Trieste, Area Science Park Basovizza, 34149 Trieste, Italy*

(Received 22 July 2015; accepted 3 November 2015; published online 23 November 2015)

In the present work, the near edge X-ray absorption spectroscopy (NEXAFS) spectra at both C and N K-edges of pyridine, 2-fluoropyridine, and 2,6-difluoropyridine have been studied both experimentally and theoretically. From an electronic point of view, both transition potential density functional theory and time-dependent density functional theory approaches lead to reliable results provided that suitable basis sets and density functionals are employed. In this connection, the global hybrid B3LYP functional in conjunction with the EPR-III basis set appears particularly suitable after constant scaling of the band positions. For the N K-edge, vertical energies obtained at these levels and broadened by symmetric Gaussian distributions provide spectra in reasonable agreement with the experiment. Vibronic contributions further modulate the band-shapes leading to a better agreement with the experimental results, but are not strictly necessary for semi-quantitative investigations. On the other hand, vibronic contributions are responsible for strong intensity redistribution in the NEXAFS C K-edge spectra, and their inclusion is thus mandatory for a proper description of experiments. In this connection, the simple vertical gradient model is particularly appealing in view of its sufficient reliability and low computational cost. For more quantitative results, the more refined vertical Hessian approach can be employed, and its effectiveness has been improved thanks to a new least-squares fitting approach. © *2015 AIP Publishing LLC.* [http://dx.doi.org/10.1063/1.4935715]

I. INTRODUCTION

Spectroscopies involving core electron transitions are useful tools to investigate complex systems: the core hole is localized on a specific site and therefore it is possible to extract information about the electronic structure of the spatial region surrounding the core-excited atom. In fact, while excitation peak positions correspond to differences between the final virtual states and the core orbital energy, the corresponding intensities (oscillator strengths) map the dipole transition moment between the two states involved in the transition. Therefore, due to the atomic nature of the initial core state and the atomic electric dipole selection rules, for K-edges the intensity actually maps the *p* contribution of the final virtual orbital on the atom carrying the core hole.

The Near Edge X-ray Absorption Spectroscopy (NEXAFS)[1] corresponds to the energetic interval of absorption near the inner-shell (or core) threshold (within 30-40 eV) where the transitions from the core orbitals to valence virtual orbitals give rise to distinct spectral features. Although these features are related to the electronic structure of the system under study, as already observed, via the electric dipole selection rules, very often their interpretation is not straightforward at all. Therefore, it is important to assist the interpretation of the experimental spectrum by means of theoretical calculations, in order to propose rationalization and assignment of the experimental spectral features being founded on a solid and reliable ground.

Up to now, various theoretical formalisms and protocols have been developed and widely applied to simulate NEXAFS spectra of big molecules and model systems, in particular with *ab initio* methods like static-exchange,[2] Density Functional Theory (DFT)[3,4] and Time Dependent DFT (TD-DFT).[5,6] In all these approaches, the most direct way to obtain the spectral intensity is to consider only the electronic contribution, by calculating the electric transition dipole moment between the initial and final bound states. On the other hand, with the concomitant continuous improvement in energy resolution of synchrotron sources and analysers, now it is possible to study the vibrational features present in NEXAFS spectra. Vibrational fine structures in NEXAFS have been identified long ago, with the first studies of ethylene by electron yield[7] and by energy loss spectra.[8] The analysis of the NEXAFS vibrational features is important, for example, to extract structural information of the excited state.[9] The theoretical

a)Author to whom correspondence should be addressed. Electronic mail: vincenzo.barone@sns.it

description of the vibrational structure in NEXAFS has been initially developed by Ågren and co-workers,[10] and is usually collected at the Linear Coupling (LC) level, which assumes only linear terms in the expansion of the final state potential around the equilibrium geometry of the initial state. In the LC model, also called Vertical Gradient (VG), vibronic effects are simulated by neglecting both mode-mixing and frequency changes between the electronic states involved in the transition. The only difference between the potential energy surfaces (PESs) of the electronic states is a shift between the equilibrium positions, which is extrapolated using the gradient of the excited state PES at the equilibrium position of the ground state. In order to check the reliability of the VG model, also the more refined Vertical Hessian (VH) model, accounting for both frequency changes and mode-mixing effects, has been tested using the general tool developed by some of us to compute vibrationally resolved electronic spectra.[11,12] The second derivatives of the excited state PES, which are required in the VH model, have been calculated using a new, general fitting procedure shortly sketched in the computational details. It is noteworthy that all the vibronic schemes are limited to core excitations to virtual bound states. When the final states lie in the continuum electronic spectrum, different methods, which consider the peculiar continuum boundary conditions, should be employed, like for example in the C1s spectrum of CF_4.[13] In that case, it has been shown that the vibrationally resolved branching ratios are sensitive to both shape resonances and diffraction effects due to the nuclei which act as scattering centers.

The present work consists of a combined experimental and theoretical analysis of the N1s and C1s NEXAFS spectra of pyridine, 2-fluoropyridine and 2,6-difluoropyridine. The electronic spectra have been considered at various levels of theory, namely, by the Transition Potential DFT (TP-DFT) scheme, where the relaxation of the core orbitals is obtained by reducing their occupation by half of an electron, and by the TD-DFT approach with a restricted excitation window. In this latter case, different global hybrid functionals (B3LYP and M06) and basis sets have been tested. For these systems, vibrational effects have been found crucial for a correct description of the C1s spectra involving strong intensity redistribution, at variance with the N K-edge, where vertical electronic transitions broadened by simple Gaussian distributions are usually sufficient.

Pyridine is an important system, since it is the simplest aromatic heterocyclic compound; moreover, its fluorinated derivatives are interesting because they include at the same time strong electronic effects related to the aromatic stabilization as well as inductive effects generated by both electronegative N and F atoms. For this reason, this series represents a challenge for theory, since it is required that all these effects are properly described in a balanced way by the adopted formalism. For pyridine in the gas phase, also previous calculations on the vibrational fine structure have been reported. It is worth noting the NEXAFS has been also employed to study not only free pyridine in the gas phase[14,15] but also when adsorbed over the silicon (110) surface, both experimentally[16] and theoretically.[17]

II. COMPUTATIONAL MODEL

A. Electronic spectra, TP-DFT

In general, within the dipole approximation, the oscillator strength for excitation from the ground state (GS) $|\Psi_g\rangle$ to the excited state $|\Psi_e\rangle$ is given by (atomic units used),

$$f_{g\to e} = \frac{2\Delta E_{g\to e}}{3}\left|\mathbf{M}_{g\to e}\right|^2, \tag{1}$$

$$\mathbf{M}_{g\to e} = \left\langle \Psi_g \left|\hat{\boldsymbol{\mu}}\right| \Psi_e \right\rangle, \tag{2}$$

where $\mathbf{M}_{g\to e}$ is the transition dipole moment, $\hat{\boldsymbol{\mu}} = \sum_i \mathbf{r}_i$ corresponds to the electric dipole operator, and $\Delta E_{g\to e} = E_e - E_g$ is the total energy difference. Taking into account the final-state rule[18–21] and the sudden approximation, Eq. (1) can be formulated at one-electron level, so that the oscillator strength is evaluated in terms of two molecular orbitals (MOs) ψ_{1s} (core) and ψ_a of the final state,

$$f_{g\to e} = \frac{2\Delta\varepsilon_{1s\to a}}{3}\left|\langle\psi_{1s}(1)\left|\mathbf{r}_1\right|\psi_a(1)\rangle\right|^2, \tag{3}$$

where $\Delta\varepsilon_{1s\to a} = \varepsilon_a - \varepsilon_{1s}$ denotes the orbital energy difference.

Structures of all systems are first optimized at the DFT level with the LDA VWN functional[22] and the Triple Zeta Polarized (TZP) basis set of Slater Type Orbitals (STOs) by using the ADF package.[23–25]

The NEXAFS spectra are calculated at the spin-restricted DFT level with the PW86 functional[26] by a locally modified version of the ADF program. The core hole at each non-equivalent center is modelled by the Half Core Hole (HCH) also referred to as the Transition Potential (TP) approximation, reducing the occupation number of the core orbital by half an electron.

The basis functions employed in the DFT-TP calculations of NEXAFS spectra consist of a very extended STO set for the core-excited atom, consisting of an even tempered Quadruple Zeta with 3 polarization and 3 diffuse functions (designated as ET-QZ3P-3DIFFUSE in the ADF database) while the TZP basis set has been employed for the remaining atoms. Symmetry is properly reduced allowing core hole localization. The raw spectra are calibrated by aligning the first transition energy $\Delta\varepsilon_{1s\to LUMO}$ (LUMO: lowest unoccupied MO) to that obtained from the ΔKohn-Sham (ΔKS) scheme,[27,28] as difference between the total energy of the excited state (E_{e_1}) and the total energy of the GS (E_g): $\Delta E_{g\to e_1} = E_{e_1} - E_g$. In order to get a pure singlet first core-excited state, E_{e_1} is computed as[29]

$$E_{e_1} = 2E\left(\left|1s\alpha^1\ldots LUMO\beta^1\right|\right) - E\left(\left|1s\alpha^1\ldots LUMO\alpha^1\right|\right). \tag{4}$$

Here, $E\left(\left|1s\alpha^1\ldots LUMO\beta^1\right|\right)$ and $E\left(\left|1s\alpha^1\ldots LUMO\alpha^1\right|\right)$ denote the total energies of two spin-polarized single-determinants with unpaired electrons in the 1s and LUMO orbitals (antiparallel and parallel, respectively). In addition, we also calculate the core Ionization Potential (IP) in the following way:

$$IP_{1s} = E\left(\left|1s\alpha^1\ldots\right|\right) - E_g, \tag{5}$$

where $E\left(\left|1s\alpha^1\ldots\right|\right)$ represents the total energy of a spin-polarized Full Core-Hole (FCH) state.

The stick spectra are broadened by using a Gaussian line-shape $\Phi(\omega;\Delta\varepsilon_{1s\to a},\gamma)$ with Half-Width-at-Half-Maximum (HWHM) $\gamma = 0.2$ eV. Finally, the atom-specific spectrum of each nonequivalent carbon center is weighted by their relative abundance and summed to get the total spectrum.

B. Electronic spectra, TD-DFT

The TD-DFT spectra have been simulated using the so-called restricted excitation window formulation (REW-TD-DFT, a description of the method can be found in Refs. 5, 30, and 31). Within the REW-TD-DFT formalism, a set of active occupied molecular orbitals is chosen, and only excitations starting from those orbitals are actually computed. This method is well suited for the calculation of the excited states involved in NEXAFS spectroscopy, since those high-energy states can be reached by including only the core orbitals in the active set. Here, for all the computations involving excitations from the N atom, only the N1s orbital has been included in the active set, whereas the 1s orbitals of equivalent carbon atoms have been treated together. Therefore, for the calculations involving excitations from the ortho and meta C atoms of pyridine and 2,6-difluoropyridine, the active range included two molecular orbitals, corresponding to linear combinations of the 1s orbitals of the equivalent C atoms.

For the TD-DFT calculations, the performance of several basis sets has been tested. The double-ζ SNSD basis set,[32] developed by some of us to provide a good balance between accuracy and computational cost in the description of spectroscopic properties of medium- and large-size molecules, has been used as a reference. To improve the description of the core orbitals, which is a mandatory requirement for the study of core excitations, also the EPR-III basis set[33] has been employed, which has been optimized for the accurate calculation of hyperfine constants. EPR-III is a triple-ζ basis set with diffuse functions and two d and one f polarization functions for the atoms from B to F. Furthermore, an additional s function is present for the atoms from B to F. To improve also the description of the valence molecular orbitals, a third basis set has been employed, referred to as EPR-IIId, which is obtained by adding diffuse polarization functions (p on hydrogen and d on atoms from B to F taken from the aug-cc-pVTZ basis set) to the EPR-III set.

C. Vibrational structure

As already remarked above, the vibrationally resolved spectra have been computed within the general theoretical framework introduced by some of us (more details can be found in Refs. 34–36) based on a time-independent (TI) formulation. To summarize, the intensity of each vibronic band is related to the transition dipole moment between the initial and final states of the transition $\langle\bar{\bar{\Psi}}|\boldsymbol{\mu}|\bar{\Psi}\rangle$, which is calculated by introducing several approximations.[36] First of all, the Born-Oppenheimer approximation is used to separate the nuclear and the electronic wave-functions, and roto-vibrational couplings are minimized by fulfilling the Eckart conditions. Under those assumptions, the transition dipole moment can be expressed as $\langle\bar{\bar{\chi}}_m|\boldsymbol{\mu}^e_{fi}|\bar{\chi}_n\rangle$, where $\bar{\chi}_n$ and $\bar{\bar{\chi}}_m$ are the vibrational levels of the initial and final electronic states involved in the vibronic transition, and $\boldsymbol{\mu}^e_{fi}$ is the electronic transition dipole moment between the initial and final electronic levels, which is in general a function of the nuclear coordinates $\mathbf{Q}$. Since no analytical expressions are available for $\boldsymbol{\mu}^e_{fi}(\mathbf{Q})$, it is usually approximated as a Taylor series around some reference geometry. In this work, only the zero-th order term (referred to as Franck-Condon term, FC), which is the leading term for fully allowed transitions, will be considered. The harmonic approximation is used then used to calculate $\bar{\chi}_n$ and $\bar{\bar{\chi}}_m$, and mode-mixing effects are included by means of the linear relation introduced by Duschinsky,

$$\overline{\mathbf{Q}} = \mathbf{J}\overline{\overline{\mathbf{Q}}} + \mathbf{K},$$

where $\overline{\mathbf{Q}}$ and $\overline{\overline{\mathbf{Q}}}$ are the normal modes of the ground and excited states, respectively, $\mathbf{J}$ is usually referred to as the Duschinsky matrix, and $\mathbf{K}$ is usually called the shift vector. Different expressions can be derived for $\mathbf{J}$ and $\mathbf{K}$, depending on the harmonic model used for the PES of the excited state. Throughout this work, vertical models will be used, in which the Taylor expansion of the PES of the excited state is performed around the equilibrium position of the ground state.[11,12,37] In the more accurate vertical model, usually referred to as Vertical Hessian (VH), both mode-mixing and frequency change effects are included in the simulation, and $\mathbf{J}$ and $\mathbf{K}$ are given by the following expressions:

$$\mathbf{J} = \overline{\mathbf{L}}^T\overline{\overline{\mathbf{L}}}, \qquad \mathbf{K} = -\overline{\overline{\mathbf{F}}}^{-1}\overline{\mathbf{L}}^{-1}\mathbf{M}^{-1/2}\overline{\overline{\mathbf{g}}},$$

where $\overline{\mathbf{L}}$ and $\overline{\overline{\mathbf{L}}}$ are the matrices with the Cartesian normal modes of the ground and excited states, respectively. Moreover, $\overline{\overline{\mathbf{g}}}$ and $\overline{\overline{\mathbf{F}}}$ are the Cartesian gradient and Hessian of the excited state PES at the equilibrium geometry of the ground state, while $\mathbf{M}$ is the diagonal matrix of the atomic masses. Despite its accuracy, the computational cost of the calculations needed to generate the input data for VH is high, since the calculation of $\overline{\overline{\mathbf{F}}}$ requires the computation of second derivatives of the excited state PES with respect to the nuclear coordinates. A significant computational saving can be achieved by neglecting mode-mixing effects ($\mathbf{J} = \mathbf{I}$) and by assuming that the frequencies of the ground state are the same as those of the excited state, since in this case only the gradient of the excited state PES is needed to compute $\mathbf{K}$. This simplified model is usually referred to as VG, and is equivalent to the so-called Linear Coupling Model (LCM).

By using all the approximations outlined above, the vibronic spectrum is expressed in terms of the overlap integrals $\langle\bar{\chi}_m|\bar{\bar{\chi}}_n\rangle$, usually referred to as Franck-Condon integrals. Within the TI approaches, those integrals are calculated explicitly using either analytical formulae or recursion relations between them. The computational tool used in this work is based on the second approach, which is more efficient and better suited for a general implementation. Furthermore, in order to reduce the computational cost of the overall procedure, a pre-screening system is used, to select

a-priori the integrals, giving the main contributions to the overall spectrum. In our implementation, a class-based pre-screening is employed, which is efficient also for large-size systems. More details regarding this procedure can be found in Refs. 11 and 12.

As remarked above, the use of the VH model requires the computation of the Hessian of the electronic excited state PES. Since the computation of energy second derivatives with respect to nuclear displacements at the REW-TD-DFT level is not yet included inside GAUSSIAN, a least-squares fitting procedure has been employed. Let us consider the local approximation of the PES about a reference structure as a Taylor expansion in terms of the Cartesian coordinates,

$$V(\mathbf{x}) \approx V(\mathbf{x}_{eq}) + \sum_{i=1}^{3N_{at}} \left(\frac{\partial V}{\partial x_i}\right)_{(eq)} x_i + \frac{1}{2} \sum_{i,j=1}^{3N_{at}} \left(\frac{\partial^2 V}{\partial x_i \partial x_j}\right)_{(eq)} x_i x_j.$$

Even if only harmonic terms have been included in the previous expansion, our general fitting procedure can be used to compute vibrational force constants at any order of derivation. In the following, for the sake of simplicity, we will refer to $\left(\partial^2 V/\partial x_i \partial x_j\right)_{(eq)}$ as k_{ij} and to $(\partial V/\partial x_i)_{(eq)}$ as k_i. As is well known, in ordinary least-squares fitting (OLS),[38,39] a function of the Cartesian coordinates $p(\mathbf{x})$ is approximated as a linear combination $p_{fit}(\mathbf{x})$ of N known basis functions $f_j(\mathbf{x})$ as follows:

$$p_{fit}(\mathbf{x}) = \sum_{j=1}^{N} a_j f_j(\mathbf{x}).$$

The coefficients a_j are obtained by calculating the value of $p(\mathbf{x})$ for M different configurations $\mathbf{x}_i$, and minimizing the difference between the values of $p_{fit}(\mathbf{s})$ and $p(\mathbf{x})$ evaluated in the sampling points, expressed by the residual function $R(\mathbf{a}) = \sum_{i=1}^{M} \left\| p(\mathbf{x}_i) - p_{fit}(\mathbf{x}_i) \right\|^2$. The solution to this problem is given by the linear system $\mathbf{Va} = \mathbf{b}$ where $\mathbf{V}$ is an $M \times N$ matrix containing the values of the basis function f_j in the sampling point $\mathbf{x}_i$, $\mathbf{b}$ is the vector with the values $p(\mathbf{s}_i)$ and $\mathbf{a}$ contains the coefficients a_j. By minimizing $R(\mathbf{a})$ with respect to the parameters a_j, the normal equation is obtained

$$(\mathbf{V^T V})\mathbf{a} = \mathbf{V^T b},$$

where $(\mathbf{V}^T\mathbf{V})$ is a square, invertible matrix. An extended least-squares method (ELS)[38,39] can be also employed, in which, together with energies also energy gradients are employed, i.e., the constants k_i are known and not included in the parameters to be fitted. Therefore, the residual function becomes

$$R(\mathbf{a}) = \sum_{i=1}^{N} \left[\left| p_{fit}(\mathbf{X}_i) - p(\mathbf{X}_i) \right|^2 + \sum_{k=1}^{3N_{at}} \left| \frac{\partial p}{\partial x_k}(\mathbf{X}_i) - \frac{\partial p_{fit}}{\partial x_k}(\mathbf{X}_i) \right|^2 \right].$$

In the case studied here, the fitted function $p(\mathbf{x})$ is the PES of the excited state and the basis functions are the second-order monomials $x_i x_j$. The grid used to select the points $\mathbf{x}_i$ is obtained by modifying individually each Cartesian coordinate with respect to its equilibrium value by a constant shift δ. Furthermore, a singular value decomposition, which is more efficient and numerically stable, has been employed to solve the normal equation.[40]

III. EXPERIMENTAL SETUP

In the present work, the NEXAFS spectra have been recorded for the substituted pyridines, whose measurements were performed at the GAs-Phase pHotoemission (GAPH) beamline of the Elettra synchrotron, in Trieste.[40]

The samples used were purchased from Sigma-Aldrich, (2-fluoropyridine C_5H_4FN 98% purity and 2,6-difluoropyridine, $C_5H_3F_2H$, 99% purity). Both samples are liquid, so it was possible to introduce their vapor in the experimental chamber through a gas line. To eliminate all traces of air and other possible contaminants, both samples were subject to several cycles of freezing and pumping *in situ*. Finally, the temperature was slowly raised and maintained at 295 K.

The NEXAFS spectra at C and N K-edges were acquired by measuring the ion yield with a channel electron multiplier placed close to the ionization region. Photon resolution was better than 70 meV at C and N K-edges. Spectra were normalized to the photon flux measured by a calibrated Si photodiode (AxVU100 IRD™).

The energy scale of the spectra was calibrated by taking simultaneous spectra of the samples and of a calibrated gas introduced into the experimental chamber. In particular, the energies of the reference peaks were 290.77 eV (C1s → π, CO_2)[41] and 401.1 eV (N1s → π, ν = 1, N_2).[42]

The calibrated experimental spectra of 2-fluoropyridine and 2,6-difluoropyridine at both C and N K-edges are reported in Figure 1.

IV. RESULTS AND DISCUSSION

A. N1s electronic spectra

In Fig. 2, the experimental N1s NEXAFS spectra of pyridine (from Ref. 14) and of its two F-derivatives (present work) measured in the gas phase are compared with the spectra computed by the TP-DFT method. The experimental profiles have been shifted on the energy scale in order to match the first intense peak ascribed to the N1s → $1\pi^*$ transition. The theoretical electronic spectra correctly describe the main features of the experiment and the energy separation among the peaks. The reproduction of both the intensity pattern and the band-shape indicates negligible vibronic effects for these transitions, as confirmed by the calculated vibronic spectra of the N1s excitations of pyridine discussed in Section IV B. We can first interpret the N1s spectra on the basis of the electronic TP-DFT results.

The first and strongest peak of the pyridine spectrum (panel a of Fig. 2) is assigned to the N1s → $1\pi^*$ ($3b_1$) transition (at 399.0 eV). The asymmetric line shape of this peak in the experiment is due to an unresolved vibrational fine structure, and in fact this asymmetry is recovered by including vibronic effects in the calculation, as discussed in the next paragraph and shown in Fig. 4. A very weak bump appears in the experiment at the higher energy side of the main peak, with an energy separation of about 1.4 eV, which is missing in the calculated spectrum. This small structure has been attributed to the N1s transition to the $2\pi^*$ orbital

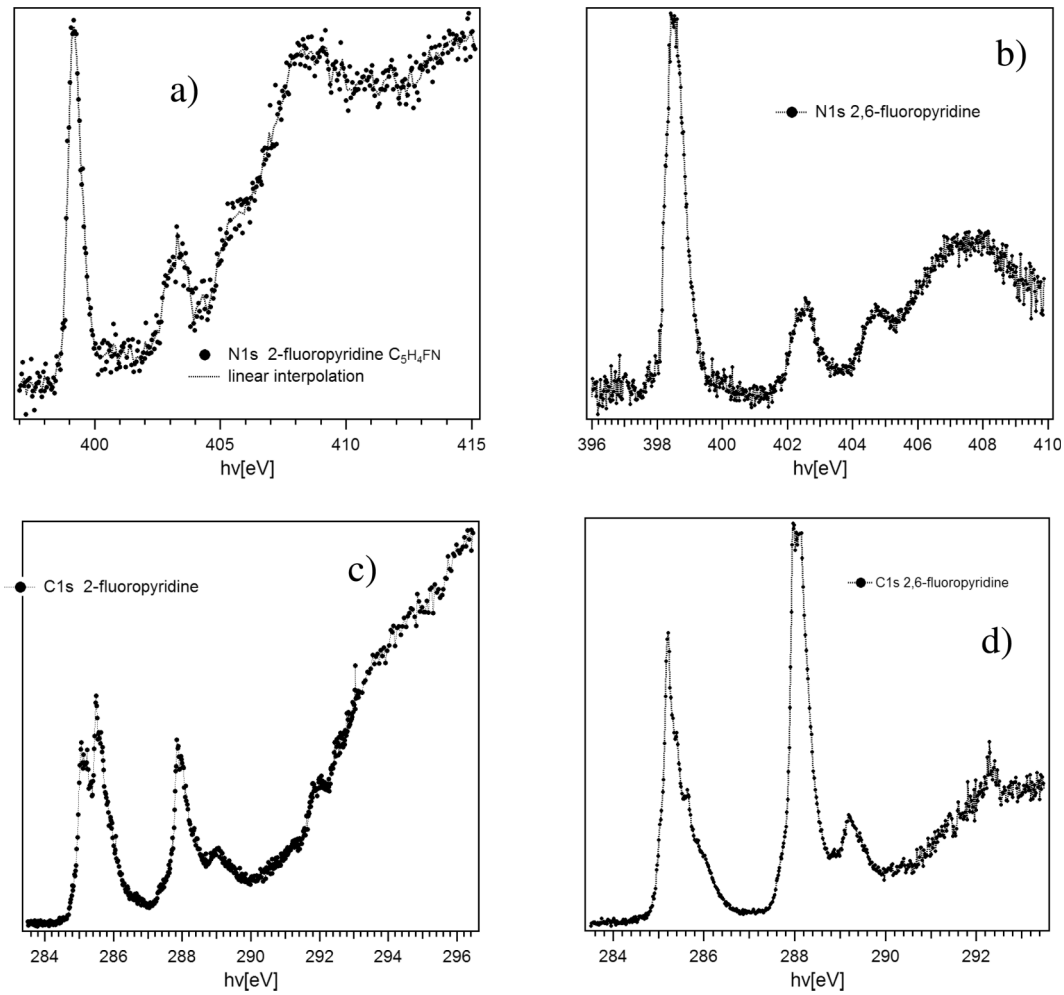

FIG. 1. The experimental NEXAFS spectra recorded in this work: (a) N1s 2-fluoropyridine, (b) N1s 2,6-difluoropyridine, (c) C1s 2-fluoropyridine, and (d) C1s 2,6-difluoropyridine.

($1a_2$), which is dipole-forbidden in C_{2v} symmetry but could obtain intensity in the experiment through vibronic coupling effects.[14] We will comment on this hypothesis in the next paragraph, where the N1s vibrational structure is discussed.

A very weak transition is calculated at 402.1 eV and assigned to an antibonding σ^*(C–H) orbital with a strong admixture of Rydberg character, in agreement with previous calculations.[14,15] It corresponds to a weak peak observed in the experiment just before the second well-defined experimental peak (around 402.6 eV on the energy scale of Fig. 2). In this energy region the calculations predict a structure which is contributed by weak transitions (around 403.0 eV) of essentially Rydberg character, followed by the more intense N1s $\rightarrow 3\pi^*$ transition (at 403.4 eV) characterized by an admixture of valence and Rydberg character. The region around the ionization threshold contains several weak transitions of mixed Rydberg and valence excitations.

The N1s spectra of the 2-fluoropyridine and 2,6-difluoropyridine reproduce the pattern of the pyridine spectrum. We observe a slight increase of the excitation energies on going from pyridine to 2,6-difluoropyridine, due to the withdrawal of the valence electron charge induced by the fluorine atoms; the energy separation among the spectral features remains however constant in the three spectra. The main peak is assigned to the N1s $\rightarrow 1\pi^*$ transition in both molecules. In the case of 2-fluoropyridine (Cs symmetry), the N1s $\rightarrow 2\pi^*$ transition is dipole-allowed and appears in the calculated spectrum at 400.2 eV. It becomes again forbidden in 2,6-difluoropyridine and is therefore not present in the spectrum. The peaks around 404 eV are mainly contributed by the N1s $\rightarrow 3\pi^*$ transition in both 2-fluoropyridine and 2,6-difluoropyridine spectra while the lower energy shoulder (at 403.0 eV in 2-fluoropyridine and 403.1 in 2,6-difluoropyridine) is assigned to a transition into an antibonding σ^*(C–H) orbital with a strong admixture of Rydberg character.

In Fig. 3, the comparison among the N1s electronic spectra of pyridine calculated at various levels of theory is reported. The TP-DFT results have been considered the target for the assessment of the best choice of the exchange correlation functionals (B3LYP and M06)[43,44] and basis sets in the TDDFT approach. Even if the M06 exchange-correlation functional in conjunction with the EPR-III basis set provides better absolute excitation energies, the relative positions of the peaks are poorly reproduced. On the other hand, a significantly better match between TP-DFT and TD-DFT results is reached with the B3LYP global hybrid functional in conjunction with the EPR-III basis set, even if the computed spectrum must be

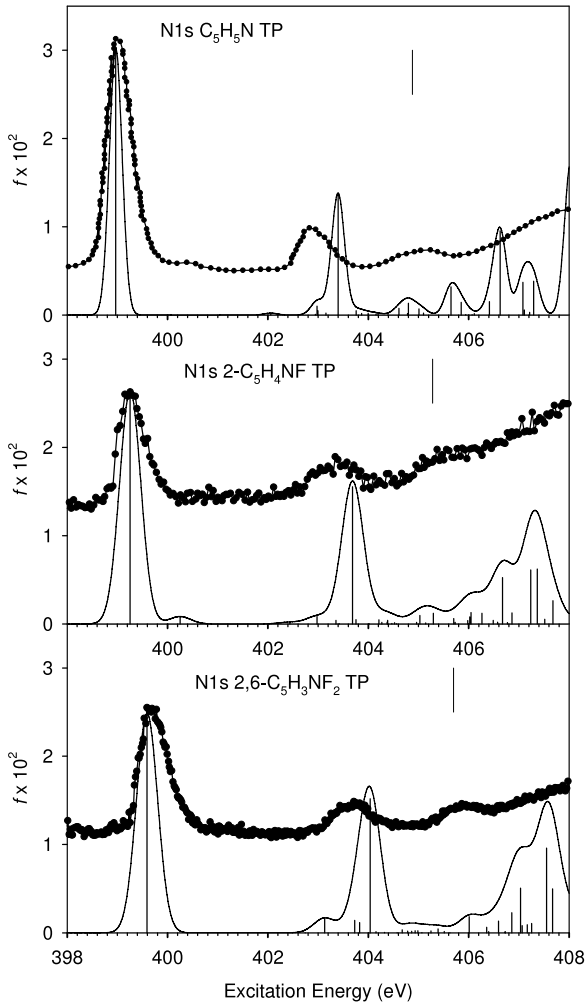

FIG. 2. N1s NEXAFS spectra of pyridine (upper panel), 2-fluoropyridine (central panel) and 2,6-difluoropyridine (lower panel): experimental data (circles) and calculated TP-DFT results (solid line and vertical bars). The computed ionization potentials are also reported. The experimental energy scale has been shifted in order to match the first calculated N1s → 1π* peak.

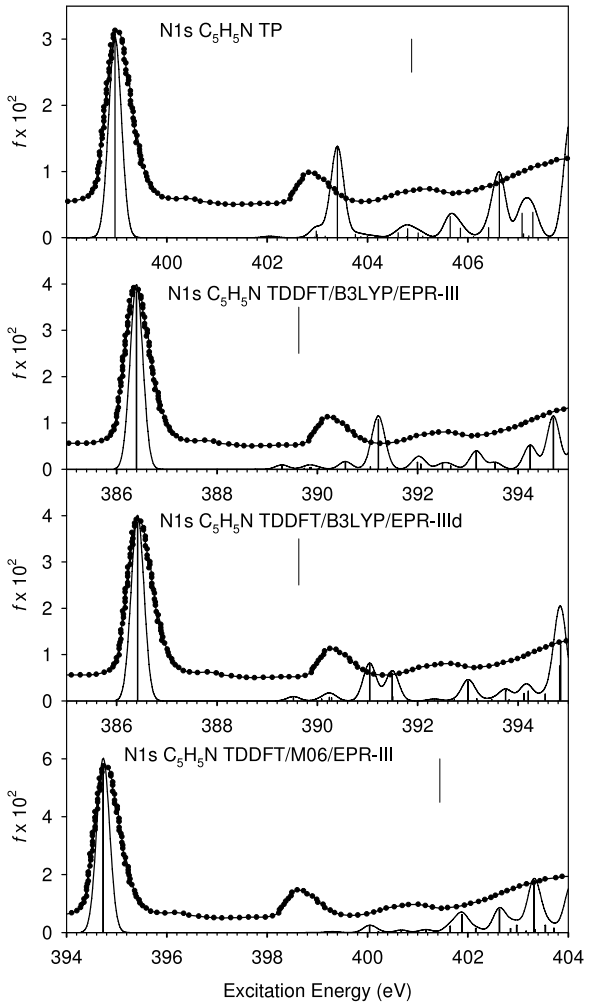

FIG. 3. N1s NEXAFS spectra of pyridine: experimental data (circles) and calculated results (solid line and vertical bars). The computed ionization potentials are also reported (for TD-DFT calculations, the absolute value of the energy of the core orbital involved in the transition is reported). Theoretical method/basis are indicated in the inset. The experimental energy scale has been shifted in order to match the first calculated N1s → 1π* peak.

shifted by about 14 eV in place of 4 eV as in the case of M06. Using the larger EPR-IIId basis set, the overall band-shape is nearly unchanged, even if slight changes are present in the high-energy region of the NEXAFS spectrum. More in detail, using the EPR-III basis set, the second peak of the experimental spectrum contains a single band, while using the EPR-IIId basis set it is composed by two overlapping, less intense bands. The agreement with the experimental data is better in this second case. Since those bands are associated with excitations to diffuse molecular orbitals, this difference is obviously related to the presence of additional diffuse basis functions in the EPR-IIId set.

B. N1s vibrational structure

In Figure 4, the experimental spectrum for the N1s excitation of pyridine is reported together with the vibronic spectrum calculated at the VG|FC level. Only the five excited states, corresponding to the highest oscillator strength in the energy range between 386 and 394 eV, have been included in the computation. By comparing the computed band-shape with the vertical energy (VE) results obtained at the TD-DFT level using the B3LYP exchange-correlation functional and the EPR-IIId basis set, reported in Figure 3, it turns out that the inclusion of vibronic effects does not change significantly the computed spectrum. In fact, both the shape and the relative intensity of the two most intense bands of the spectrum, located at about 386 and 392 eV, are nearly unchanged with respect to the results, obtained at the VE level. In order to study the vibronic effects on the forbidden N1s → 2π* ($1a_2$) transition, a VH model including Herzberg-Teller effects has been employed. The calculated intensities for the vibronic transitions are much weaker (about three orders of magnitude) with respect to those of the N1s → 1π* transition and are not able to change the shape of the main band when they are summed up to the vibronic transitions of the first peak. Therefore, we are led to conclude that the vibronic coupling is not able to increase appreciably the intensity of the dipole forbidden N1s → 2π* ($1a_2$) transition in pyridine, which we expect not to be detectable. As a consequence, the weak structure reported in the experiment of

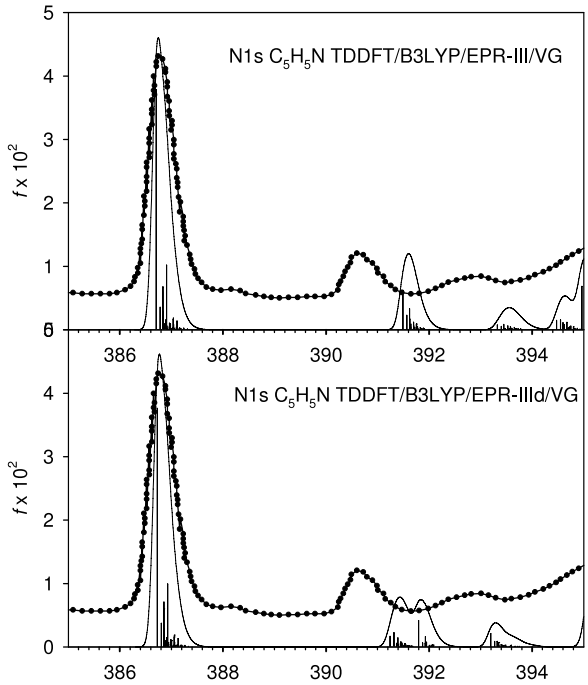

FIG. 4. N1s NEXAFS spectra of pyridine: experimental and calculated results including vibronic effects at the VG level (solid line and vertical bars). Theoretical method/basis are indicated in the inset.

Ref. 14 assigned to N1s → $2\pi^*$ ($1a_2$) is probably an artefact of the noisy background. This observation is further supported by a more recent experiment[15] which does not show any feature related to the N1s → $2\pi^*$ ($1a_2$) transition. Moreover, the energy resolution for N1s NEXAFS is 90 meV in Ref. 15, which is better than 150 meV reported in Ref. 14.

C. C1s electronic spectra

In Figure 5, the C1s excitation spectrum of pyridine calculated with different methods is compared with the experiment, the latter having been shifted on the energy scale in order to match the first C1s → $1\pi^*$ transition of the calculation. Starting with the TP-DFT scheme (upper panel), the calculated total C1s spectrum is characterized by a sharp double-peak band around 286 eV followed by weaker features starting around 288 eV and reaching a maximum around 290 eV. The theory reproduces only qualitatively the experiment, in fact the relative intensity of the double-peak feature at 286 eV (in the experiment the first peak is less intense than the second one) is reversed in the calculation. The double peak-structure of the first band can be rationalized taking into account the different contributions to the total absorption. In fact, the band is ascribed to the three different C1s → LUMO ($1\pi^*$) transitions; therefore the relative excitation energies reflect the relative energy of the core orbitals: the ortho C1s feels the proximity of the electronegative N atom, which depletes electron density, then the ortho C1s orbital is less shielded and concomitantly more bounded to the nucleus and therefore a larger excitation energy is predicted for the ortho C1s. Such an effect, which corresponds to an energy difference of 0.5 eV, is in remarkable agreement with the experiment. It is worth noting that in the ortho and meta partial profiles

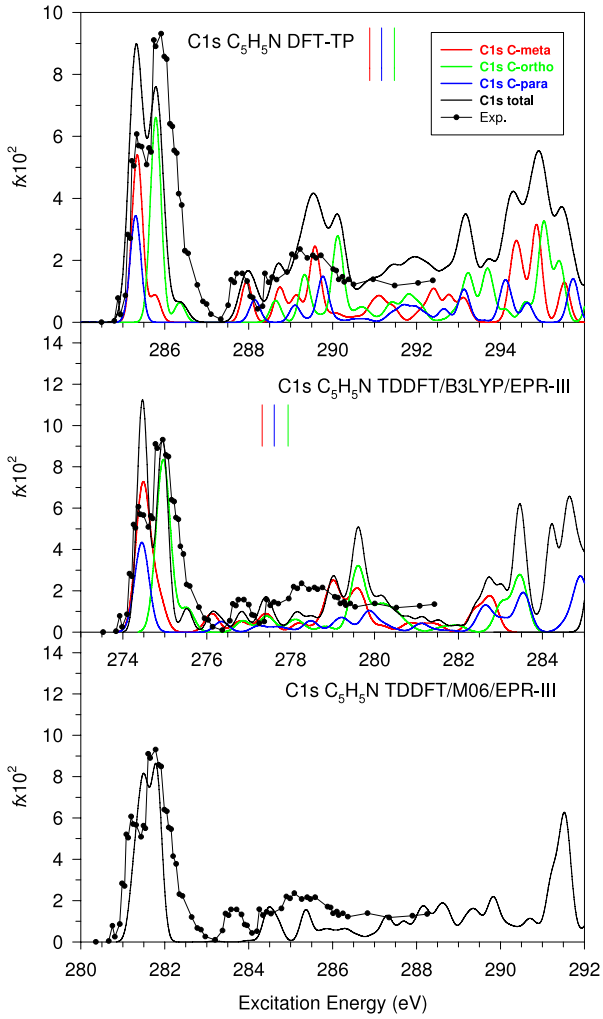

FIG. 5. C1s NEXAFS spectra of pyridine: experimental data (circles) and calculated results (solid line). The computed ionization potentials are also reported (for TD-DFT calculations, the absolute value of the energy of the core orbital involved in the transition is reported). Theoretical method/basis are indicated in the inset and partial contributions in the legend. The experimental energy scale has been shifted in order to match the first calculated C1s → $1\pi^*$ peak.

a weak secondary maximum is observed, at 286.3 eV and 285.8 eV, respectively, those transitions being ascribable to excitations to the $2\pi^*$ orbital. Such a feature is absent in the para partial profile because $2\pi^*$ has a nodal plane orthogonal to the molecular plane passing through the N and para C atoms; therefore its dipole transition moment vanishes due to symmetry constraints. The $1\pi^*$ and $2\pi^*$ orbitals derived from the $1\pi^*$ degenerate orbital of benzene (e_{2u} in D_{6h}), which, due to symmetry lowering (to C_{2v}) split to b_1 ($1\pi^*$) and a_2 ($2\pi^*$) orbitals in pyridine. The highest valence virtual $3\pi^*$ orbital (corresponding to the b_{2g} one of benzene) lies much higher in energy and contributes to the transitions around 290 eV. This high-energy region, however, is rather complicated, since it encompasses transitions to many final virtual orbitals, including σ^*(C–H) antibonding orbitals as well as diffuse Rydberg states. Although this spectral region is extremely congested, preventing a detailed assignment of all the calculated spectral features, the calculation is in good agreement with the experiment. In summary, a comparison

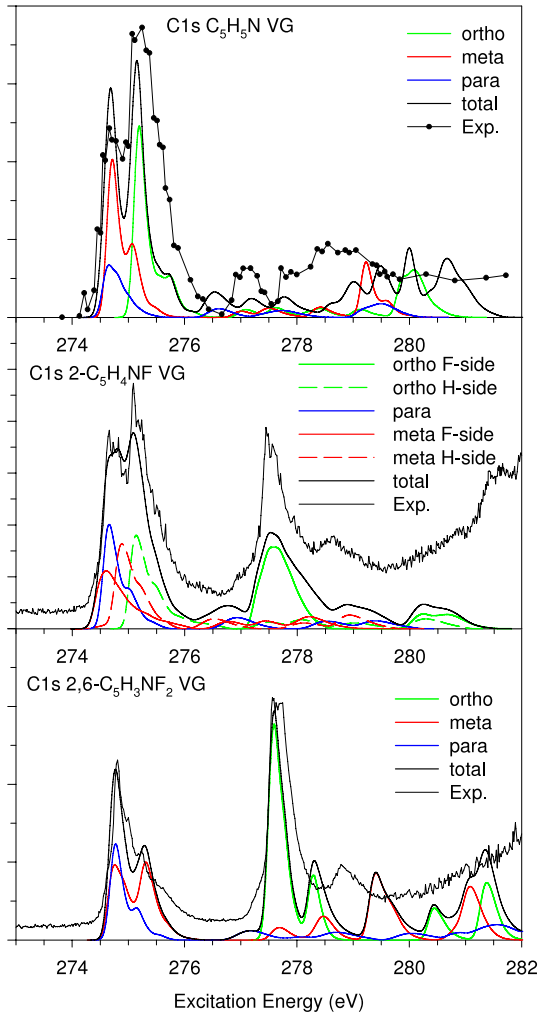

FIG. 6. C1s NEXAFS spectra of pyridine (upper panel), 2-fluoropyridine (central panel) and 2,6-difluoropyridine (lower panel): experimental data (circles) and calculated results (solid line) including vibronic coupling at the VG level. Theoretical method/basis are indicated in the inset and partial contributions in the legend. The experimental energy scale has been shifted in order to match the first calculated C1s → $1\pi^*$ peak.

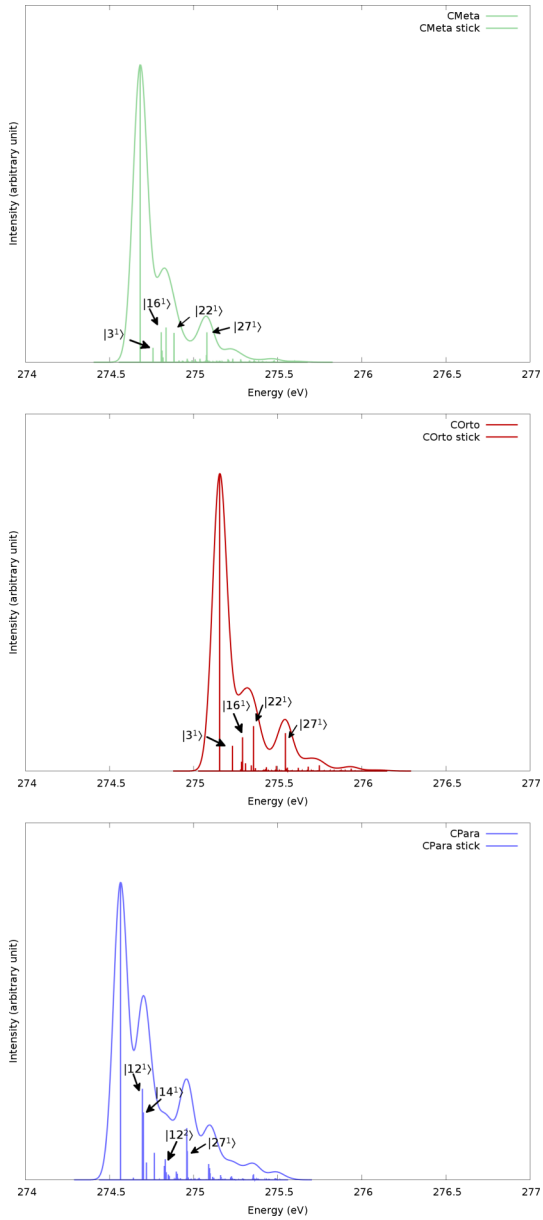

FIG. 7. Vibronic C1s NEXAFS spectra of pyridine for excitations from the meta (upper panel), ortho (middle panel) and para (lower panel) carbon atoms. The VG|FC model has been used to simulate vibronic effects. Gaussian distribution functions with a HWHM of 0.05 eV have been used to simulate broadening effects. The assignment of the most intense transition is also reported in the figure.

between the TP-DFT electronic calculations and experiment is fully satisfactory as far as the relative excitation energies are concerned, but if the intensity distribution is considered, an inversion is found for the first band at 286 eV. This disagreement is very intriguing, since it might be ascribed to different causes, like a problem in the description of the spectrum caused by a deficiency in the electronic structure or, more likely, the neglect of vibrational effects in the computational model.

For this reason, we have been led to investigate this problem in more detail considering a different approach to calculate the electronic spectrum. We have selected the TD-DFT method for two reasons: (1) it is a well established and accurate method to describe core electron excitation and (2) TD-DFT supports the calculation of the vibrational effects. In the central and lower panels of Figure 5, the electronic C1s spectrum of pyridine has been calculated at the TD-DFT level, employing two different exchange-correlation energy functionals (B3LYP and M06) in conjunction with the EPR-III basis set.[33] The B3LYP results are very similar to the TP-DFT ones, and the reversed energy distribution is found also in this case for the double-peak first band, whose analysis in terms of partial contributions matches perfectly with that obtained with the TP-DFT scheme. This finding suggests that the disagreement with the experiment should not be ascribed to problems with the electronic structure but rather to the absence in the calculation of vibrational effects. In the lower panel of Figure 5, the M06 functional is considered, as already observed for the N1s excitation the comparison with the experiment is even worse. From such an analysis it can be concluded that the B3LYP functional is adequate to describe accurately the C1s excitation spectrum at the TD-DFT level of theory, and that the vibrational effects can be added starting with this scheme.

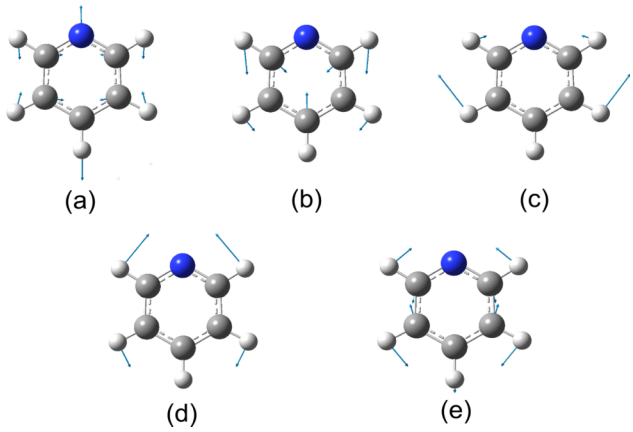

FIG. 8. Graphical representation of the normal modes of pyridine, giving the most intense vibronic transitions in the calculated C1s NEXAFS spectrum.

D. C1s vibrational structure

In the upper panel of Figure 6, the vibronic spectrum calculated at the VG|FC level for C1s excitations in pyridine in the range between 274 and 281 eV is shown together with the experimental results. The 28 excited states corresponding to the largest oscillator strength (11 associated with excitations from the 1s C ortho orbitals, 11 from the 1s C meta ones and 7 from the 1s C para) have been included in the computation. In this case, remarkable differences are present with respect to the theoretical results both at the TP-DFT level and at the TD-DFT level, reported in Figure 5. Let us consider, for example, the double-peak structure present in the low energy range of the spectrum (see the upper panel of Figure 5 at about 286 eV). As already remarked in Sec. IV C, this pattern is poorly reproduced at the vertical energy level, since

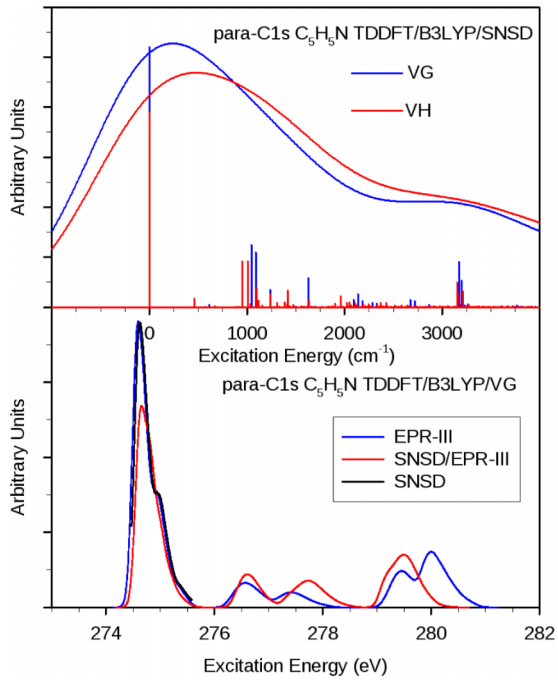

FIG. 9. Comparison between different levels of vibronic coupling (VG/VH) and basis sets (EPR-III and SNSD) on the vibronic spectra of para C1s in pyridine.

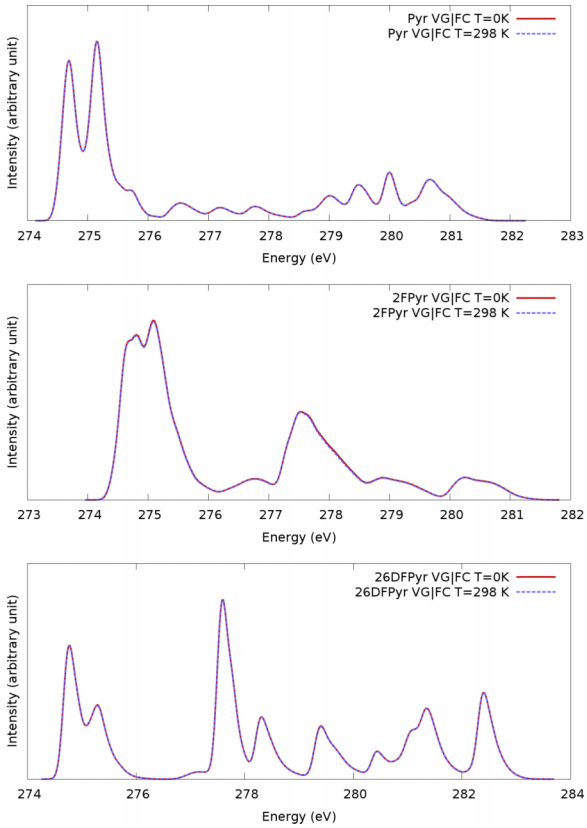

FIG. 10. Vibronic NEXAFS spectra of pyridine (upper panel), 2-fluoropyridine (middle panel) and 2,6-difluoropyridine (lower panel) for excitations from the C1s orbitals calculated at the VG|FC level at 0 K (solid, red line) and at 298 K (dashed, blue line). Broadening effects have been simulated using Gaussian functions with a HWHM of 0.1 eV.

the intensity of the first peak is expected to be larger than that of the second one. However, the inclusion of vibronic effects modifies the relative intensities of the two peaks, and a better match with the experimental results is reached. In order to analyze this effect in deeper detail, the vibronic NEXAFS spectra for excitations from the C1s orbital of each non-equivalent C atom to the $1\pi^*$ virtual orbital are shown separately in Figure 7. Even if the vibronic band-shapes are nearly equivalent for the excitations starting from the C1s orbitals of the ortho and meta atoms, a larger number of intense vibronic transitions are present for the spectrum associated with the para C1s $1\pi^*$ excitation. Therefore, the transition between the vibrational ground states of the two PESs (usually referred to as 0-0 transition) is less intense with respect to the other ones and the vibronic broadening is significantly larger. Due to polarization effects, the band associated with the para C1s $1\pi^*$ transition lies in the low-energy region of the double peak signal, and therefore the relative intensity of the first sub-peak decreases, giving a better match with the experimental results. For the sake of completeness, in Figure 8 a graphical representation of the normal modes giving intense vibronic transitions is reported. It is noteworthy that the active normal modes are associated with in-plane deformations of the ring, since the extrapolated equilibrium geometry of the excited states associated with bright transitions is, in every case, planar, and therefore vibronic transitions involving out-of-plane deformations are inactive.

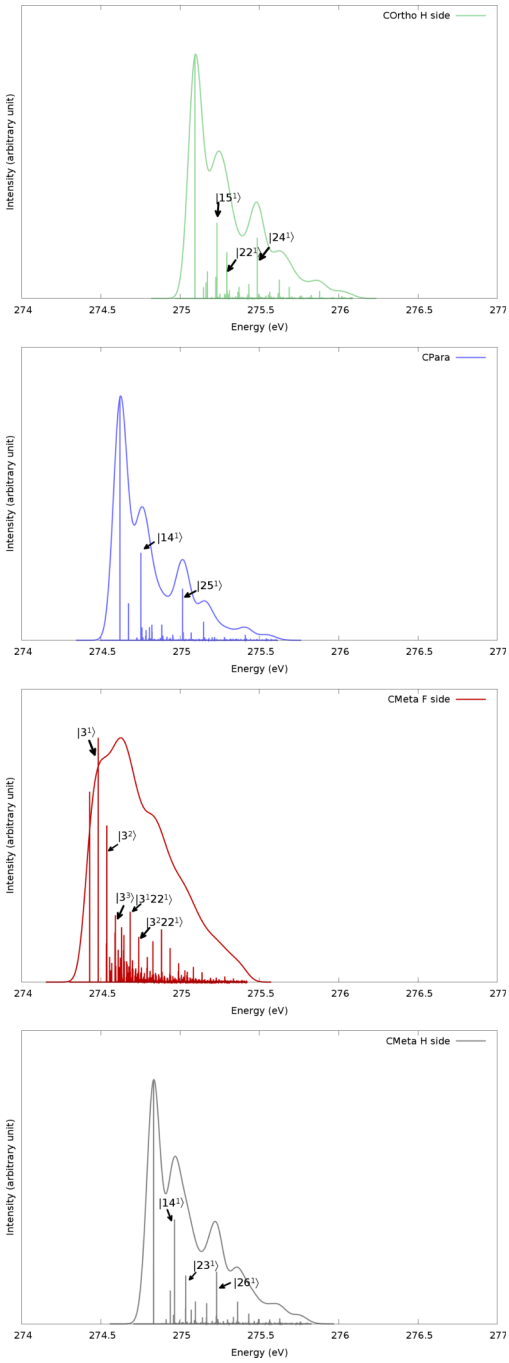

FIG. 11. Vibronic C1s NEXAFS spectra of 2-fluoropyridine for excitations from the C ortho H side (upper panel), para (middle, upper panel) meta F side (middle, lower panel) and meta H side (lower panel) carbon atoms. The VG|FC model has been used to simulate vibronic effects. Gaussian distribution functions with a HWHM of 0.05 eV have been used to simulate broadening effects. The assignment of the most intense transition is also reported in the figure.

The spectrum associated with the para C1s $1\pi^*$ transition of pyridine has been chosen also as a test case to check the reliability of the VG model to describe vibronic effects. In fact, even if this model has been already used to simulate vibronic NEXAFS spectra,[45,14] a comparison with the results obtained with more refined vibronic models is, to the best of our knowledge, still lacking. For this purpose, the theoretical spectrum has been simulated also at the VH|FC level, therefore

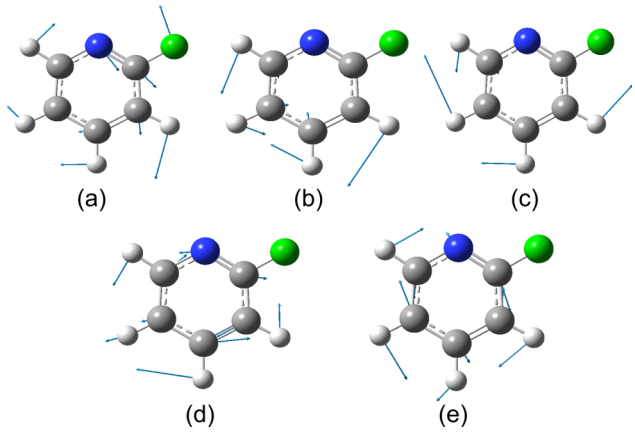

FIG. 12. Graphical representation of the normal modes of 2-fluoropyridine giving the most intense vibronic transitions in the calculated C1s NEXAFS spectrum.

including mode-mixing effects. As already discussed in Sec. II C, the Hessian matrix of the excited state PES used to compute **J** has been calculated using a least squares fitting procedure. In Figure 9 both the VG|FC and the VH|FC spectra for the para C1s $1\pi^*$ transition are reported. It is noteworthy that the inclusion of mode-mixing effects does not modify significantly the overall band-shape. The only differences between the two spectra are an overall shift of the spectrum, as well as a shift of each vibronic band toward lower energy. In fact, in the VH model, the exact frequencies of the excited state are used instead of those of the ground state, and therefore both the zero-point vibrational energy and the position of the vibronic transitions change. Since the results obtained using the two different models are nearly equivalent, in the following the simpler VG one will be used in all the simulations.

For purposes of completeness, we have investigated also temperature effects. In fact, even if all the previous computations have been performed at 0 K, therefore by assuming that the starting level is the vibrational ground state of the initial state PES, the experimental spectra have been recorded at 298 K. Temperature effects have been included in the vibronic simulations within the time-independent formalism (TI) following the procedure outlined in Ref. 46, and including in the computation all the vibrational levels of the ground electronic state with a Boltzmann population larger than 0.1. The results sketched in the upper panel of Figure 10 show that, as expected for such rigid systems, the spectra calculated at 0 K and 298 K are nearly superimposable, and therefore temperature effects do not affect significantly the computed band-shape.

The vibronic spectra, calculated at the VG|FC level, for the C1s NEXAFS spectrum of 2-fluoropyridine are reported in the middle panel of Figure 6, together with the shifted experimental spectrum. In this case, the 27 excited states associated with the largest value of the oscillator strength have been included in the simulation. As for pyridine, also in this case the low-energy region of the experimental spectrum is characterized by a double-peak structure, where the first peak is less intense than the second one. As shown in Figure 6, this spectral pattern is well reproduced by including vibronic

effects. As already done previously for pyridine, in Figure 11 the vibronic spectra for the C1s $1\pi^*$ excitations for each non-equivalent C atom are reported separately. Let us recall that the carbon directly bonded to the fluorine atom gives a signal at significantly higher energy due to polarization effects, and therefore it is not included in Figure 11. Comparison of those spectra shows that the vibronic band-shape is similar for three of them, except for the excitation from the C meta atom lying on the same side of the F, giving a significantly broader spectrum. More in detail, for the first three spectra, only few vibronic transitions (whose assignment is reported in the spectrum) have a noticeable intensity, and therefore the broadening of the spectrum is limited. On the other hand, for the fourth excitation, a larger number of intense vibronic peaks can be identified, and also several overtones and combination bands are active and therefore the spectrum is significantly broader. The spectrum associated with the excitation from the 1s orbital of the C Meta atom lying on the F side to the $1\pi^*$ orbital contributes to the low-energy sub-peak of the double-peak structure present in the experimental spectrum; the inclusion of vibronic effects decreases the relative intensity of this peak, therefore giving a better reproduction of the experimental results. Also in this case, a graphical representation of the normal modes, giving the largest vibronic transitions, is reported in Figure 12. In analogy with pyridine, also in this case the extrapolated equilibrium geometries of all excited electronic states are planar, and therefore only in plane normal modes are active. Also in this case temperature effects have been investigated and, as shown in the middle panel of Figure 10, their inclusion does not modify the overall band-shape.

In conclusion, the NEXAFS vibronic spectrum for 2,6-difluoropyridine simulated at the VG|FC level is reported in the lower panel of Figure 6. The 34 excited states associated with the largest oscillator strength have been included in the simulation (10 for excitations from the C ortho atom, 14 from the C meta one and 10 from the C para). As for the excitation spectrum from the 1s orbital of the N atom in pyridine, also in this case the inclusion of vibronic effects does not affect significantly the simulated band-shape. In fact, the shapes of the two most intense peaks of the experimental spectrum (at about 275 and 278 eV) are nearly unchanged with respect to their VE counterparts, even if the intensity of the first band decreases slightly. A more relevant difference is present in the energy region above 279 eV, where the inclusion of vibronic effects leads to an overall intensity decrease for all the bands, thus giving a better matching with the experimental results. As shown in the lower panel of Figure 10, also for this system temperature effects are negligible.

V. CONCLUSIONS

In the present work, the NEXAFS spectra at both C and N K-edges of pyridine, 2-fluoropyridine and 2,6-difluoropyridine have been studied both experimentally and theoretically. It has been shown that for the N K-edge TP-DFT vertical energy computations are accurate enough for a general description of the spectrum as well as for the assignment of the most relevant features. Vibrational effects have been found to be important only for a proper description of the shape of the peaks, but are not strictly necessary. On the other hand, in the NEXAFS C K-edge spectra the vibronic effects are responsible for strong intensity redistribution, so their inclusion has proven necessary for an accurate description of the experiment. In any case, the VG|FC treatment of the vibronic couplings has proven adequate, so that more complete schemes as VH are not necessary for an accurate description of K-edge NEXAFS. Also temperature effects have shown to be negligible.

ACKNOWLEDGMENTS

This work has been supported by MIUR (PRIN 2010) of Italy. Generous CINECA ISCRA grants for computer time at CINECA (Bologna, Italy) are gratefully acknowledged.

[1]J. Stöhr, *NEXAFS Spectroscopy* (Springer Verlag, Berlin, Heidelberg, New York, 1992).
[2]H. Ågren, V. Carravetta, O. Vahtras, and L. G. M. Pettersson, Chem. Phys. Lett. **222**, 75 (1994).
[3]G. Fronzoni, R. De Francesco, and M. Stener, J. Phys. Chem. A **116**, 2885 (2012).
[4]L. Triguero, L. G. M. Pettersson, and H. Ågren, Phys. Rev. B **58**, 8097 (1998).
[5]M. Stener, G. Fronzoni, and M. de Simone, Chem. Phys. Lett. **373**, 115 (2003).
[6]N. A. Besley and F. A. Asmuruf, Phys. Chem. Chem. Phys. **12**, 12024 (2010).
[7]W. Eberhardt, R. P. Haelbich, M. Iwan, E. E. Koch, and C. Kunz, Chem. Phys. Lett. **40**, 180 (1976).
[8]A. P. Hitchcock and C. E. Brion, J. Electron Spectrosc. Relat. Phenom. **10**, 317 (1977).
[9]Y. Ma, F. Sette, G. Meigs, S. Modesti, and C. T. Chen, Phys. Rev. Lett. **63**, 2044 (1989).
[10]O. Plashkevych, T. Privalov, H. Ågren, V. Carravetta, and K. Ruud, Chem. Phys. **260**, 11 (2000).
[11]V. Barone, J. Bloino, M. Biczysko, and F. Santoro, J. Chem. Theory Comput. **5**, 540 (2009).
[12]J. Bloino, M. Biczysko, F. Santoro, and V. Barone, J. Chem. Theory Comput. **6**, 1256 (2010).
[13]M. Patanen, K. Kooser, L. Argenti, D. Ayuso, M. Kimura, S. Mondal, E. Plesiat, A. Palacios, K. Sakai, O. Travnikova, P. Decleva, E. Kukk, C. Miron, K. Ueda, and F. Martin, J. Phys. B: At., Mol. Opt. Phys. **47**, 124032 (2014).
[14]C. Kolczewski, R. Püttner, O. Plashkevych, H. Ågren, V. Staemmler, M. Martins, G. Snell, A. S. Schlachter, M. Sant'Anna, G. Kaindl, and L. G. M. Pettersson, J. Chem. Phys. **115**, 6426 (2001).
[15]G. Vall-Llosera, G. Gao, A. Kivimäki, M. Coreno, J. Álvarez Ruiz, M. de Simone, H. Ågren, and E. Rachlew, J. Chem. Phys. **128**, 044316 (2008).
[16]R. Coustel, S. Carniato, F. Rochet, and N. Witkowski, Phys. Rev. B **85**, 035323 (2012).
[17]M. Romeo, G. Balducci, M. Stener, and G. Fronzoni, J. Phys. Chem. C **118**, 1049 (2014).
[18]U. von Barth and G. Grossman, Solid State Commun. **32**, 645 (1979).
[19]U. von Barth and G. Grossmann, Phys. Rev. B **25**, 5150 (1982).
[20]T. Privalov, F. Gel'mukhanov, and H. Ågren, Phys. Rev. B **64**, 165115 (2001).
[21]T. Privalov, F. Gel'mukhanov, and H. Ågren, Phys. Rev. B **64**, 165116 (2001).
[22]S. H. Vosko, L. Wilk, and M. Nusair, Can. J. Phys. **58**, 1200 (1980).
[23]G. te Velde, F. M. Bickelhaupt, E. J. Baerends, C. Fonseca Guerra, S. J. A. van Gisbergen, J. G. Snijders, and T. Ziegler, J. Comput. Chem. **22**, 931 (2001).
[24]C. Fonseca Guerra, J. G. Snijders, G. te Velde, and E. J. Baerends, Theor. Chem. Acc. **99**, 391 (1998).
[25]E. J. Baerends, T. Ziegler, J. Autschbach, D. Bashford, A. Bárces, F. M. Bickelhaupt, C. Bo, P. M. Boerrigter, L. Cavallo, D. P. Chong *et al.*, ADF2010, SCM, Theoretical Chemistry, Vrije Universiteit, Amsterdam, The Netherlands, 2010, http://www.scm.com.
[26]J. P. Perdew, Phys. Rev. B **33**, 8822 (1986).
[27]P. S. Bagus, Phys. Rev. **139**, 619 (1965).
[28]L. Triguero, O. Plashkevych, L. G. M. Pettersson, and H. Ågren, J. Electron Spectrosc. Relat. Phenom. **104**, 195 (1999).
[29]T. Ziegler, A. Rauk, and E. J. Baerends, Theor. Chim. Acta **43**, 261 (1977).
[30]W. Liang, S. A. Fischer, M. J. Frisch, and X. Li, J. Chem. Theory Comput. **7**, 3540 (2011).

[31]P. J. Lestrange, P. D. Nguyen, and X. Li, J. Chem. Theory Comput. **11**, 2994 (2015).
[32]V. Barone, P. Cimino, and E. Stendardo, J. Chem. Theory Comput. **4**, 751 (2008).
[33]V. Barone, in *Recent Advances in Density Functional Methods, Part I*, edited by D. P. Chong (World Scientific Publishing Company, Singapore, 1996).
[34]V. Barone, A. Baiardi, M. Biczysko, J. Bloino, C. Cappelli, and F. Lipparini, Phys. Chem. Chem. Phys. **14**, 12404 (2012).
[35]A. Baiardi, J. Bloino, and V. Barone, J. Chem. Theory Comput. **9**, 4097 (2013).
[36]M. Biczysko, J. Bloino, F. Santoro, and V. Barone, in *Computational Strategies for Spectroscopy: From Small Molecules to Nano Systems*, edited by V. Barone (John Wiley & Sons, Chichester, UK, 2011), pp. 361–826.
[37]A. Hazra, H. H. Chang, and M. Nooijen, J. Chem. Phys. **121**, 2125 (2004).
[38]P. Carbonniere, D. Begue, A. Dargelos, and C. Pouchan, Chem. Phys. **300**, 41 (2004).
[39]P. Carbonniere, D. Begue, and C. Pouchan, Chem. Phys. Lett. **393**, 92 (2004).
[40]R. Blyth, R. Delaunay, M. Zitnik, J. Krempasky, R. Krempaska, J. Slezak, K. Prince, R. Richter, M. Vondracek, R. Camilloni, L. Avaldi, M. Coreno, G. Stefani, C. Furlani, M. de Simone, S. Stranges, and M.-Y. Adam, J. Electron Spectrosc. Relat. Phenom. **101–103**, 959 (1999).
[41]M. Tronc, G. C. King, and F. H. Read, J. Phys. B: At. Mol. Phys. **12**, 137 (1979); **13**, 999 (1980).
[42]R. N. S. Sodhi and C. E. Brion, J. Electron Spectrosc. Relat. Phenom. **34**, 363 (1984).
[43]C. Lee, W. Yang, and R. G. Parr, Phys. Rev. B **37**, 785 (1988).
[44]Y. Zhao and D. Truhlar, Theor. Chem. Acc. **120**, 215 (2008).
[45]G. Fronzoni, O. Baseggio, M. Stener, W. Hua, G. Tian, Y. Luo, B. Apicella, M. Alfé, M. de Simone, A. Kivimäki, and M. Coreno, J. Chem. Phys. **141**, 44313 (2014).
[46]F. Santoro, A. Lami, R. Improta, J. Bloino, and V. Barone, J. Chem. Phys. **128**, 224311 (2008).